Applied Catalysis B: Environmental 154–155 (2014) 379–385

Contents lists available at ScienceDirect

Applied Catalysis B: Environmental

journal homepage: www.elsevier.com/locate/apcatb

# Characterization and photoactivity of coupled ZnO–$ZnWO_4$ catalysts prepared by a sol–gel method

Abdessalem Hamrouni[a,b], Noomen Moussa[a], Agatino Di Paola[b,*], Francesco Parrino[b], Ammar Houas[a,c], Leonardo Palmisano[b]

[a] Unité de Recherche Catalyse et Matériaux pour l'Environnement et les Procédés URCMEP (UR11ES85), Faculté des Sciences de Gabès/Université de Gabès, Campus Universitaire Cité Erriadh, Gabès 6072, Tunisie
[b] "Schiavello-Grillone" Photocatalysis Group, Dipartimento di Energia, Ingegneria dell'Informazione e Modelli Matematici (DEIM), Università di Palermo, Viale delle Scienze, Palermo 90128, Italy
[c] Al Imam Mohammad Ibn Saud Islamic University (IMSIU), College of Sciences, Department of Chemistry, Riyadh 11623, Saudi Arabia

ARTICLE INFO

*Article history:*
Received 7 December 2013
Received in revised form 18 February 2014
Accepted 22 February 2014
Available online 3 March 2014

*Keywords:*
Photocatalysis
ZnO–$ZnWO_4$ nanocomposites
Sol–gel method
Coupled semiconductors

ABSTRACT

ZnO–$ZnWO_4$ nanocomposites were synthesized by a novel sol–gel method and characterized through X-ray diffraction, BET specific surface area analysis, UV–Vis diffuse reflectance spectroscopy, scanning electron microscopy and transmission electron microscopy. The photocatalytic activity of the samples was evaluated using the degradation of 4-nitrophenol under UV light as probe reaction. The ZnO/$ZnWO_4$ molar ratio was varied in order to study its influence on the photoefficiency of the mixed samples. The ZnO–$ZnWO_4$ nanocomposites showed higher photoactivity than ZnO and $ZnWO_4$. The high efficiency of the mixed samples was explained by the coupling and the intimate contact of two different semiconductors having suitable energy levels of their conduction and valence bands that allow an improved charge separation of the photogenerated electron–hole pairs.



## 1. Introduction

In the last two decades, heterogeneous photocatalysis has been the focus of a considerable attention in green chemistry, fine chemicals and in emerging "Advanced Oxidation Processes" (AOPs) [1–3] especially for air and water remediation [4].

When a photocatalyst is excited with photons of energy equal or higher than its band gap energy, electrons ($e^-$) and holes ($h^+$) pairs are created. In an aqueous or gaseous medium, reactants can react either with electrons or with holes. A good photocatalyst should adsorb reactants and absorb light efficiently preferably in the visible or near UV region of the electromagnetic spectrum.

Zinc oxide (ZnO) has been broadly studied as a photocatalyst due to its photosensitivity, and its attractive optoelectronic and catalytic properties. In many studies, ZnO was found efficient for the decomposition of many non-biodegradable organic compounds [5–9] due to the position of its valence band that gives a strong oxidizing power to the photogenerated holes. However, the photocatalytic activity of ZnO is limited by the recombination reaction of the photogenerated electron/hole pairs that reduces the efficiency of the photocatalytic processes.

Coupling different semiconductors allows the vectorial displacement of electrons from one semiconductor to another, leading to a more efficient electron/hole separation and greater catalytic reactivity [10]. ZnO has been coupled to various semiconductors such as ZnO–$TiO_2$ [11–13], ZnO–CdS [14,15], ZnO–$SnO_2$ [16–21] to improve its photocatalytic activity. Only few publications have concerned the synthesis of ZnO–$ZnWO_4$ [22,23] and ZnO–$ZnWO_4$–$WO_3$ [24] photocatalysts to be employed for the photodegradation of organic compounds.

Zinc tungstate ($ZnWO_4$) is a promising material for applications in heterogeneous photocatalysis due to its interesting physical and chemical properties [25–39]. Zhu and coworkers reported that $ZnWO_4$ exhibited relatively high photocatalytic activity for the degradation of aqueous solutions of rhodamine B [25–31] and methylene blue [30,37] and also for gaseous formaldehyde [26–28]. $ZnWO_4$ was efficient for the decomposition of salicylic acid [35] and the decoloration of methyl orange [37], malachite green [36,38] and rhodamine 6G [33]. Up to now $ZnWO_4$ photocatalysts have been synthesized by a variety of different processes including co-precipitation [26], hydrothermal methods [28–33], microwave assisted techniques [35,39] and mechanochemical synthesis at room temperature [38].

* Corresponding author. Tel.: +39 091 238 63729; fax: +39 702 5020.
*E-mail addresses:* hamrouni-28@hotmail.fr (A. Hamrouni), agatino.dipaola@unipa.it (A. Di Paola).

http://dx.doi.org/10.1016/j.apcatb.2014.02.042
0926-3373/

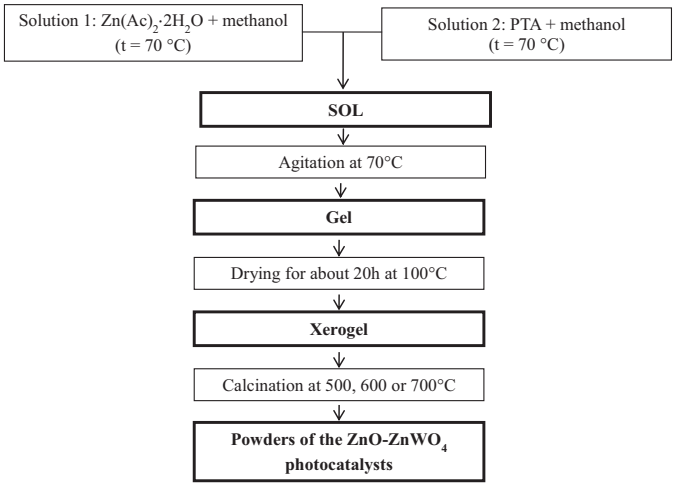


**Fig. 1.** Flowchart of the synthesis of the ZnO–$ZnWO_4$ photocatalysts.

In the present paper we report the synthesis of $ZnWO_4$ and ZnO–$ZnWO_4$ photocatalysts obtained by a novel sol–gel method. The photocatalytic activity of the samples was evaluated using the degradation of 4-nitrophenol (4-NP) chosen as a probe molecule because substituted phenols are ubiquitous contaminants in water streams [40]. The influence of the ZnO/$ZnWO_4$ molar ratio and the calcination temperature was investigated. Photovoltage measurements were also carried out to seek a correlation between the relative positions of the energy bands of ZnO and $ZnWO_4$ and the photocatalytic activity of the coupled catalysts.

## 2. Experimental

### 2.1. Synthesis

Zinc acetate dihydrate (Sigma–Aldrich), phosphotungstic acid hydrate (Sigma–Aldrich) and methanol were used as received without any further purification.

The ZnO–$ZnWO_4$ mixed photocatalysts were synthesized according to the flowchart presented in Fig. 1. Solution 1 and solution 2 were prepared by dissolving $Zn(Ac)_2{\cdot}2H_2O$ and $H_3PW_{12}O_{40}{\cdot}xH_2O$ (PTA) in methanol under stirring at 70 °C. Amounts of $Zn(Ac)_2{\cdot}2H_2O$ and PTA corresponding to an equal number of Zn and W atoms were used to prepare pure $ZnWO_4$. The amounts of precursors were opportunely determined in order to obtain powders with molar ratios ZnO/$ZnWO_4$ equal 1/0.02, 1/0.05, 1/0.25. The samples were labeled ZnO, Zn–$ZW_{0.02}$, Zn–$ZW_{0.05}$, Zn–$ZW_{0.25}$, and $ZnWO_4$. Solution 1 was added slowly to solution 2 and the mixture was aged for about 2 h to obtain the sol. The natural pH of the sol was always about 5 whatever the molar ratio. A gel was formed by stirring the sol for some hours at 70 °C. Then, the obtained gel was dried for about 20 h at 100 °C to produce the xerogel. Finally, the photocatalysts were obtained by calcining the xerogel for 2 h at different temperatures (500, 600 or 700 °C). Pure ZnO was synthesized by using only $Zn(Ac)_2{\cdot}2H_2O$ as the precursor.

### 2.2. Characterization

X-ray diffraction patterns of the powders were recorded at room temperature by an Ital Structures APD 2000 powder diffractometer using the Cu Kα radiation and a 2$\theta$ scan rate of 2°/min.

The mean grain size of the photocatalysts was estimated using the Debye–Scherrer equation:

$$D = 0.9\lambda/\beta\cos\theta \quad (1)$$

where $D$ is the mean grain size (nm), $\lambda$ is the wavelength of the X-ray radiation (0.154 nm), $\beta$ is the corrected full width at half maximum height and $\theta$ is the diffraction angle. The specific surface area (SSA) of the samples was determined with a Micrometrics Flow Sorb 2300 instrument by using the single-point BET method. UV–Vis diffuse reflectance spectra (DRS) of the samples were recorded by using a Shimadzu UV-2401PC spectrophotometer. $BaSO_4$ was used as a reference and the spectra were recorded in the range 200–800 nm.

The morphology of the catalysts was examined using a Philips XL30 ESEM scanning electron microscope (SEM), operating at 30 kV on specimens upon which a thin layer of gold was deposited. Transmission electron microscopy (TEM) measurements were obtained using a JEM-2100 (JEOL, Japan) operating at 200 kV accelerating voltage, equipped with an energy dispersive X-ray spectrometer (EDS, Oxford, UK) suitable for element identification. The powders were dispersed in isopropanol and a small drop was deposited on a 200 mesh carbon-coated copper grid, which was introduced into the TEM chamber analysis after complete solvent evaporation.

### 2.3. Photovoltage measurements

Photovoltage measurements were performed in a Pyrex reactor with a total volume of 150 mL. 100 mg of the photocatalyst were added to 100 mL of a 0.1 M $NaNO_3$ solution. A platinum electrode was used as working electrode and the reference was an Ag/AgCl electrode. After degassing for 30 min with $N_2$, 20 mg of methyl viologen (1,1′-dimethyl-4,4′-bipyridinium dichloride) were added to the suspension. Then, the mixture was once more degassed for 30 min. The pH was adjusted using $HNO_3$ and NaOH solutions. During the experiments the suspension was irradiated by two UV lamps (Philips HPK 125 W). The values of pH and potential ($V$) were measured using a pH meter Thermo Orion 720A and a multimeter Metex 3800, respectively.

### 2.4. Photocatalytic experiments

A cylindrical Pyrex batch photoreactor containing 0.15 L of the 4-NP solution (20 mg/l) was used to perform the photodegradation experiments. For each photocatalytic run the amount of photocatalyst was chosen in order to ensure that almost all the photons emitted by the lamp were adsorbed by the suspension. The photon flux was measured using a radiometer (Delta Ohm DO9721 with a UVA probe). The light source was a 125 W medium pressure Hg lamp (Helios Italquartz, Italy) with a maximum emission at about 365 nm, axially positioned within the photoreactor. The temperature of the suspension was controlled by circulation of water through a Pyrex thimble surrounding the lamp. A magnetic stirrer was used to guarantee the homogeneity of the reacting mixture. Before the light was turned on, the suspension was kept in the dark for 2 h to reach the adsorption–desorption equilibrium. Samples were taken at different time intervals to evaluate the progress of the 4-NP degradation. Each sample was filtered by a 0.2 μm filter and the residual 4-NP concentration was measured by the UV–Vis spectrophotometer.

After the photocatalytic run, the powders were sometimes recuperated, washed with distilled water and a fresh solution of 4-NP was added to test the reusability of the catalysts.

## 3. Results

### 3.1. Structural and morphological characterization

Fig. 2 shows the X-ray patterns of the photocatalysts calcined at 600 °C for 2 h. Pure ZnO, $ZnWO_4$ and mixed ZnO–$ZnWO_4$ samples were obtained with the present sol–gel protocol. The main

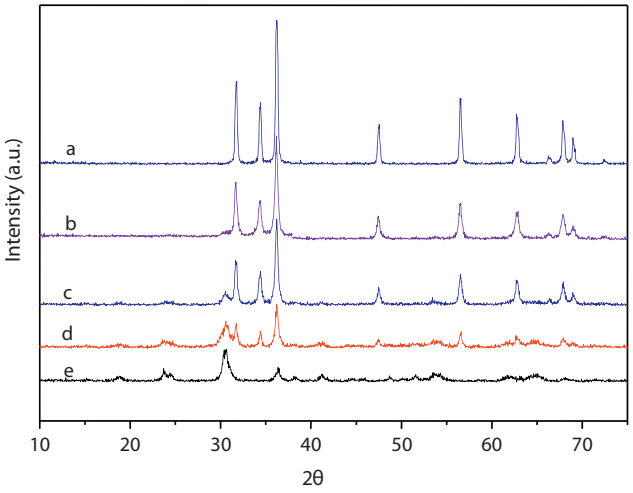


**Fig. 2.** XRD patterns of (a) ZnO, (b) Zn–$ZW_{0.02}$, (c) Zn–$ZW_{0.05}$, (d) Zn–$ZW_{0.25}$ and (e) $ZnWO_4$ calcined at 600 °C for 2 h.

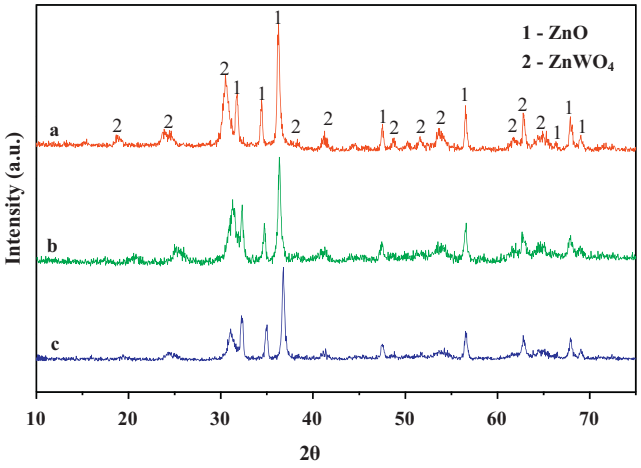


**Fig. 3.** XRD patterns of Zn–$ZW_{0.25}$ calcined for 2 h at different temperatures: (a) 700 °C, (b) 600 °C and (c) 500 °C.

peaks were indexed corresponding to hexagonal ZnO (JCPDS card number: 36-1451) and monoclinic $ZnWO_4$ (JCPDS card number: 15-0774). The peaks of pure $ZnWO_4$ were broad and not well defined, due to a low crystallinity. The peaks related to $ZnWO_4$ were detected in Zn–$ZW_{0.25}$ but were very small for Zn–$ZW_{0.05}$ and just appreciable for Zn–$ZW_{0.02}$. No characteristic peaks of other compounds such as $WO_3$ were observed.

Fig. 3 shows representative X-ray patterns of Zn–$ZW_{0.25}$ samples calcined for 2 h at 500, 600 or 700 °C. The peaks of both phases became sharper with increasing temperature indicating a growth of the size of the particles. These results are in good accordance with the measurements of specific surface area whose values decreased from 27.3 $m^2/g$ at 500 °C to 12.6 $m^2/g$ at 700 °C.

The average grain sizes of the various samples determined by using the diffraction peaks (1 0 1) for ZnO and (1 1 1) for $ZnWO_4$ are reported in Table 1. The crystal size of ZnO in the ZnO–$ZnWO_4$ samples was lower than that determined for pure ZnO indicating that the presence of $ZnWO_4$ inhibits the growth of the ZnO particles. As shown in Table 1 the specific surface areas of the mixed photocatalysts were higher than those of pure ZnO or $ZnWO_4$.

The surface morphology of the samples has been analyzed by SEM and HR-TEM images. Fig. 4 shows SEM micrographs of pure ZnO, pure $ZnWO_4$ and Zn–$ZW_{0.05}$ calcined at 600 °C for 2 h. All the samples consisted of aggregates of particles whose average sizes

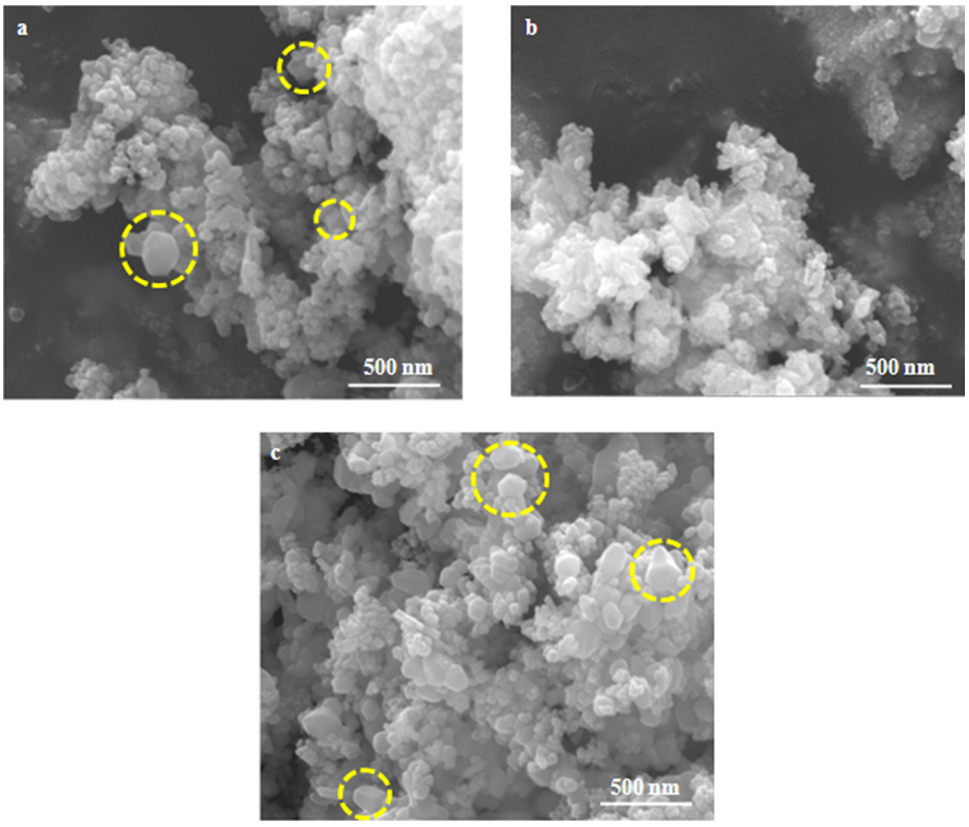


**Fig. 4.** SEM micrographs of (a) ZnO, (b) $ZnWO_4$ and (c) Zn–$ZW_{0.05}$.

**Table 1**
Physical characteristics of pure ZnO, pure $ZnWO_4$ and ZnO–$ZnWO_4$ nanocomposites.

| | ZnO 600 °C/2 h | $ZnWO_4$ 600 °C/2 h | $ZnZW_{0.02}$ 600 °C/2 h | $ZnZW_{0.05}$ 600 °C/2 h | $ZnZW_{0.25}$ 500 °C/2 h | $ZnZW_{0.25}$ 600 °C/2 h | $ZnZW_{0.25}$ 700 °C/2 h |
|---|---|---|---|---|---|---|---|
| Mean size of ZnO (nm) | 30.0 | – | 26.1 | 26.2 | 23.3 | 26.1 | 26.2 |
| Mean size of $ZnWO_4$ (nm) | – | 12.0 | – | 12.1 | 9.1 | 11.4 | 12.1 |
| SSA ($m^2/g$) | 4.3 | 12.9 | 18.0 | 19.7 | 27.3 | 18.6 | 12.6 |
| Band gap (eV) | 3.20 | 3.14 | 3.21 | 3.22 | 3.23 | 3.23 | 3.22 |

appeared quite close to those calculated from the XRD patterns. As shown in Fig. 4a, the particles of pure ZnO had a hexagonal-like shape (a small number of hexagons are indicated by circles) whereas the particles of $ZnWO_4$ (Fig. 4b) were rather irregular. The micrographs of the mixed ZnO/$ZnWO_4$ samples revealed the presence of both morphologies. Fig. 4c shows the representative SEM image of $ZnZW_{0.05}$. As highlighted by circles, the small crystallites of the different phases were interwoven with each other forming tightly bound nanoclusters.

Fig. 5 shows HR-TEM images of $ZnZW_{0.25}$ calcined at 600 °C for 2 h. The sample was composed of nanoparticles with sizes in the range of about 70–150 nm (Fig. 5a) and each nanoparticle was attached to several other nanoparticles. Fig. 5b reveals the formation of a junction between two nanoparticles with different morphologies. As shown in Fig. 5c, the energy dispersive spectroscopy (EDS) analysis confirmed that the sample consisted of Zn and W elements (copper came from the grid of the sample holder) which is consistent with the XRD results.

### 3.2. DRS spectroscopy

Fig. 6 shows the UV–Vis absorption spectra of the various samples. All the photocatalysts were responsive in the ultraviolet region but pure $ZnWO_4$ exhibited a very low intensity probably due to its poor crystallinity.

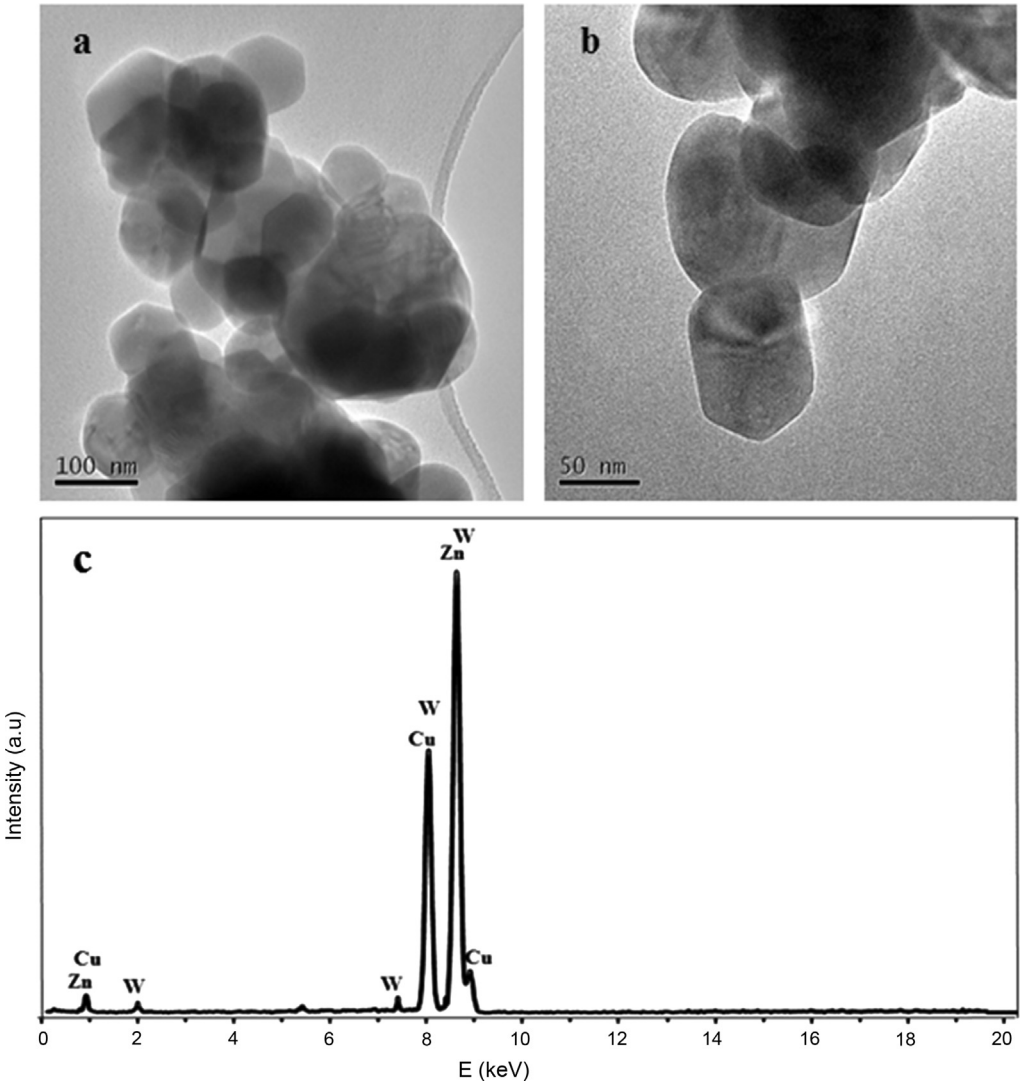


**Fig. 5.** (a, b) TEM images and (c) EDS spectrum of Zn–$ZW_{0.25}$.

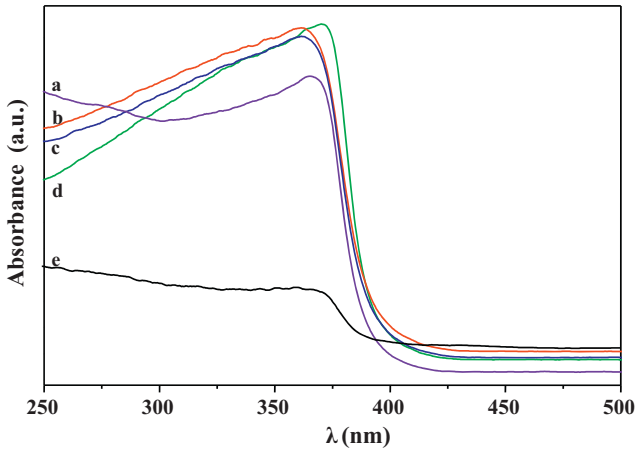


**Fig. 6.** UV–vis absorption spectra of (a) Zn–$ZW_{0.25}$, (b) Zn–$ZW_{0.02}$, (c) Zn–$ZW_{0.05}$, (d) ZnO and (e) $ZnWO_4$.

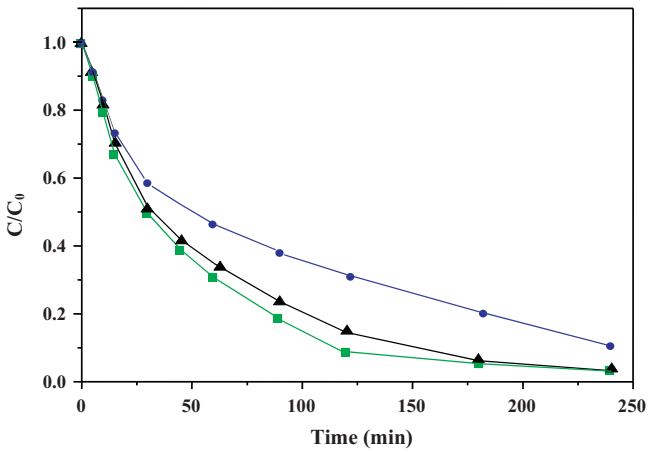


**Fig. 8.** Photodegradation kinetics of 4-NP over Zn–$ZW_{0.25}$ calcined for 2 h at (●) 500 °C, (■) 600 °C and (▲) 700 °C.

The band gap values ($E_g$) of the photocatalysts were estimated by extrapolation of the linear part of the plots of $(\alpha h\nu)^2$ versus the energy of the exciting light assuming that all the samples were direct crystalline semiconductors [41]. As shown in Table 1, the $E_g$ values of ZnO and $ZnWO_4$ were 3.20 and 3.14 eV, respectively. The band gap values of the samples containing ZnO and $ZnWO_4$ ranged between 3.21 and 3.23 eV and were scarcely dependent on the ZnO–$ZnWO_4$ ratio.

### 3.3. Photovoltage measurements.

The values of the flat band potential ($E_{FB}$) of the ZnO and $ZnWO_4$ samples were determined by the slurry method proposed by Roy et al. [42], measuring the variation of the photovoltage with the pH of suspensions of the powders in the presence of an electron acceptor. Fig. 7 shows the photovoltage vs pH curves obtained by irradiation of ZnO and $ZnWO_4$ suspensions in the presence of methyl viologen dichloride. The pH value of the inflection point ($pH_0$) of the obtained sigmoidal curves allows calculating the flat band potential at pH 7 by the equation:

$$E_{FB}(pH = 7) = E^0_{MV^{2+}/MV^{+\bullet}} + 0.059(pH_0 - 7). \quad (2)$$

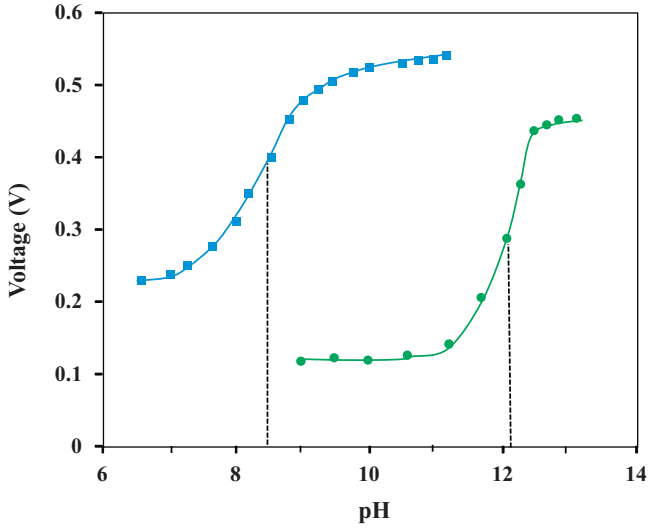


**Fig. 7.** Effect of pH on the photovoltage developed by irradiation of (■) pure ZnO and (●) pure $ZnWO_4$ calcined at 600 °C for 2 h.

where $E^0_{MV^{2+}/MV^{+\bullet}}$ is the standard potential of the redox couple $MV^{2+}/MV^{+\bullet}$ equal to −0.445 V vs (NHE) [43]. The values obtained were −0.36 V vs (NHE) for ZnO and −0.14 V vs (NHE) for $ZnWO_4$.

### 3.4. Photocatalytic activity

The photocatalytic activity of the powders was investigated by following the degradation of 4-NP under UV light irradiation. Figs. 8 and 9 show the kinetics of photodegradation of 4-NP in the presence of various samples. The degradation rate constant, $k$, was calculated from the initial slope of the concentration versus time profiles. The $k$ values are reported in Table 2.

Fig. 8 shows the effect of the calcination temperature on the photocatalytic activity of the $ZnSn_{0.25}$ sample. The best efficiency was obtained when the sample was calcined at 600 °C whereas the powders calcined at 500 and 700 °C were less active. As reported by Ohtani et al. [44] for $TiO_2$ photocatalysts, a high activity should satisfy two requirements: large surface area to adsorb the substrates and high crystallinity to reduce the recombination of the photoexcited electron–hole pairs. The sample calcined at 500 °C has the highest SSA (27.3 $m^2/g$) but it is the least crystalline. Instead, the sample calcined at 700 °C has a high crystallinity but it has a low specific surface area (12.6 $m^2/g$) so that $ZnZW_{0.25}$ calcined at 600 °C was the most active among the three samples.

Fig. 9 shows the kinetics of degradation of 4-NP in the presence of ZnO, $ZnWO_4$ and mixed ZnO–$ZnWO_4$ photocatalysts calcined for

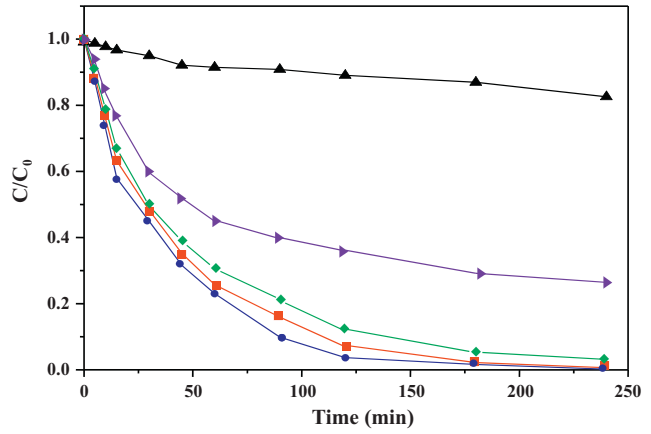


**Fig. 9.** Photodegradation kinetics of 4-NP over (●) $ZnZW_{0.05}$, (■) $ZnZW_{0.02}$, (♦) $ZnZW_{0.25}$, (►) pure ZnO and (▲) pure $ZnWO_4$ calcined at 600 °C for 2 h.

**Table 2**
Photodegradation rate constants of 4-NP on pure ZnO, pure $ZnWO_4$ and ZnO–$ZnWO_4$ photocatalysts.

| | ZnO 600 °C/2 h | $ZnWO_4$ 600 °C/2 h | $ZnZW_{0.02}$ 600 °C/2 h | $ZnZW_{0.05}$ 600 °C/2 h | $ZnZW_{0.25}$ 500 °C/2 h | $ZnZW_{0.25}$ 600 °C/2 h | $ZnZW_{0.25}$ 700 °C/2 h |
|---|---|---|---|---|---|---|---|
| $k \times 10^3$ ($min^{-1}$) | 16.5 | 2.3 | 33.6 | 36.3 | 13.6 | 25.8 | 24.8 |

2 h at 600 °C. The photoactivity of $ZnWO_4$ was very low compared to that of ZnO but all the ZnO–$ZnWO_4$ samples were more active than the two pure compounds showing that the contemporaneous presence of ZnO and $ZnWO_4$ resulted in a synergistic effect. The photocatalytic activity of the mixed samples was found to be related to the ZnO/$ZnWO_4$ molar ratio and in particular, $ZnZW_{0.05}$ revealed the highest photocatalytic efficiency.

The stability of the ZnO–$ZnWO_4$ samples was tested by XRD analysis before and after the photoreaction. The intensities of the peaks of ZnO and $ZnWO_4$ remained practically unchanged indicating the absence of photo-corrosion. Fig. 10 shows the results obtained after reuse of ZnO and $ZnZW_{0.05}$. Although the degradation efficiency of the mixed sample slightly decreased, $ZnZW_{0.05}$ was again more efficient than ZnO indicating that the ZnO–$ZnWO_4$ photocatalysts remained effective and reusable under UV light irradiation.

## 4. Discussion

The experimental results have shown that the photocatalytic activity of ZnO is increased by coupling with $ZnWO_4$. This enhancement can be explained by the contemporaneous presence of two semiconductors possessing different energy levels for their corresponding conduction and valence bands. Depending on the potentials of the photogenerated holes and electrons, a vectorial transfer of charge carriers from a semiconductor to another is possible, leading to more efficient electron–hole separation and higher photocatalytic activity [10,45].

Both ZnO and $ZnWO_4$ are n-type semiconductors so that, assuming that the difference between flat band potential and conduction band edge is negligible, it is possible to locate the valence band edge of ZnO and $ZnWO_4$ by adding the band gap energy to the flat-band potential value. The results have shown that the valence band of ZnO ($E_{VB}$ = 2.84 eV) is lower than that of $ZnWO_4$ ($E_{VB}$ = 3.00 eV). Similarly, the conduction band of ZnO ($E_{CB}$ = −0.36 eV) is lower than that of $ZnWO_4$ ($E_{CB}$ = −0.14 eV). Fig. 11 shows a schematic diagram of the energy band structures of ZnO and $ZnWO_4$ at pH = 7. Although these data may not be the exact absolute values of the conduction and valence band potentials of ZnO and $ZnWO_4$, they should offer a correct estimation of the relative band edge positions of the two semiconductors.

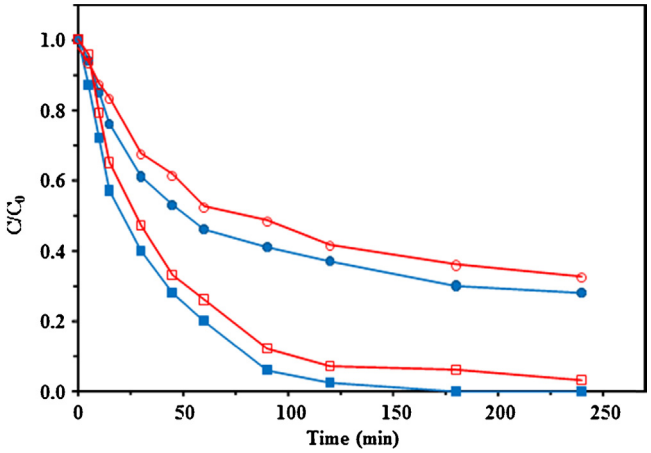


**Fig. 10.** Reusability tests of (●, ○) ZnO and (■, □) $ZnZW_{0.05}$. The full symbols refer to the first photocatalytic run, the open symbols to the second one.

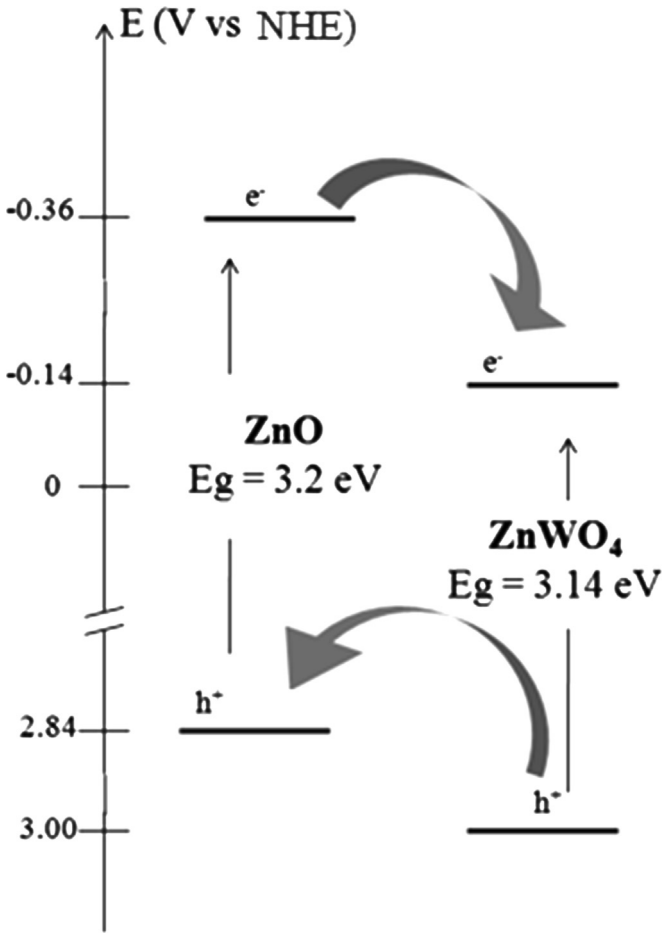


**Fig. 11.** Schematic diagram representing the charge-transfer processes between coupled ZnO and $ZnWO_4$ particles.

When the ZnO–$ZnWO_4$ nanocomposites are irradiated by UV light, electrons can transfer from the more cathodic conduction band of ZnO to the more anodic conduction band of $ZnWO_4$. Analogously, holes transfer can occur from the valence band of $ZnWO_4$ to the valence band of ZnO. The efficient charge separation can increase the lifetime of the charge carriers and enhance the efficiency of the interfacial charge transfer to adsorbed substrates. A mechanistic scheme of the charge separation in the ZnO–$ZnWO_4$ system is shown in Fig. 11.

The enhanced photoactivity of the ZnO–$ZnWO_4$ nanocomposites is so attributable to the formation of local heterojunctions between ZnO and $ZnWO_4$ particles which facilitate the separation of the photogenerated $e^-/h^+$ pairs. With increase in the content of $ZnWO_4$ the photoactivity increases due to the an increased number of heterojunctions but it decreases when the content of $ZnWO_4$ is high probably due to a larger amount of free $ZnO_4$ particles that are not sufficiently active. Therefore, there is an optimum $ZnWO_4$ content that leads to a maximum photocatalytic efficiency.

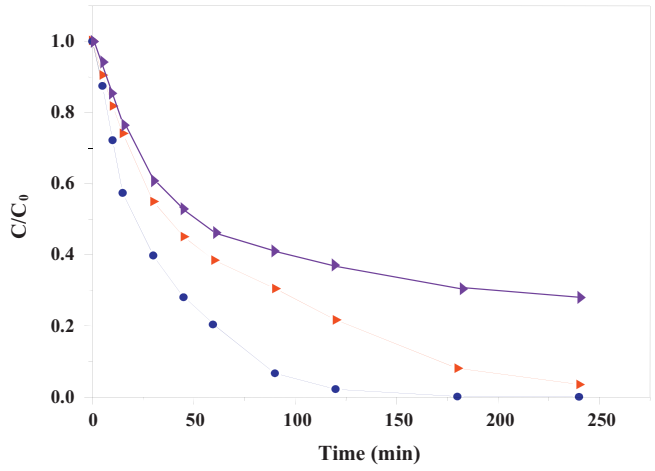


**Fig. 12.** Photodegradation kinetics of 4-NP over (▶) pure ZnO, (●) $ZnZW_{0.05}$ calcined at 600 °C for 2 h and (▶) mechanical mixture of ZnO and $ZnWO_4$.

To verify if the superior activity of the mixed systems was due to the simple coupling of different semiconductors, the photodegradation of 4-NP was also studied in the presence of a mechanical mixture of ZnO and $ZnWO_4$. Fig. 12 shows a comparison between the results obtained with the $ZnZW_{0.05}$ sample synthesized by the sol–gel method and in the presence of a mechanical mixture with the same composition. The efficiency of this mixture was superior to that of ZnO but lower than that exhibited by the ZnO–$ZnWO_4$ nanocomposite. This may be explained by assuming that an intimate contact between ZnO and $ZnWO_4$ particles is necessary for an acceleration of the rate of 4-NP degradation under illumination. Such intimate contact between different particles is easily realized during the sol–gel synthesis of the ZnO–$ZnWO_4$ nanocomposites while for the mechanical mixture of the powders, there is only a temporary juxtaposition of two distinctly separated phases.

## 5. Conclusion

ZnO, $ZnWO_4$ and ZnO–$ZnWO_4$ nanocomposites were successfully synthesized by a novel sol–gel method followed by calcination. $Zn(Ac)_2{\cdot}2H_2O$, $H_3PW_{12}O_{40}{\cdot}xH_2O$ and methanol were used as the precursors materials. The XRD patterns confirmed the presence of ZnO and $ZnWO_4$ and the absence of $WO_3$. The photoefficiency of the ZnO–$ZnWO_4$ samples was superior to that of pure ZnO or $ZnWO_4$. The enhanced photoactivity was attributed to the improved charge separation resulting from the coupling of two semiconductors with different energy levels of their conduction and valence bands. The photocatalytic activity was found to be dependent on the calcination temperature and on the ZnO/$ZnWO_4$ molar ratio. $ZnZW_{0.05}$ revealed the highest efficiency for the degradation of 4-NP.

## Acknowledgements

This work was financially supported by MIUR (Rome). HR-TEM experimental data were provided by Centro Grandi Apparecchiature – UniNetLab – Università di Palermo funded by P.O.R. Sicilia 2000–2006, Misura 3.15 Quota Regionale. The authors thank the minister of Higher Education and Scientific Research, Tunisia, for the fellowship awarded to A. Hamrouni.

## References

[1] A. Houas, H. Lachheb, M. Ksibi, E. Elaloui, C. Guillard, J.M. Herrmann, Appl. Catal. B: Environ. 31 (2001) 145–157.
[2] J.M. Hermann, J. Photochem. Photobiol. A: Chem. 216 (2010) 85–93.
[3] K. Nakata, A. Fujishima, J. Photochem. Photobiol. C: Photochem. Rev. 13 (2012) 169–189.
[4] A. Di Paola, E. García-López, G. Marcì, L. Palmisano, J. Hazard. Mater. 211 (2012) 3–29.
[5] M. Miyauchi, A. Nakajima, T. Watanabe, K. Hashimoto, Chem. Mater. 14 (2002) 2812–2816.
[6] E. Yassitepe, H.C. Yatmaz, C. Öztürk, K. Öztürk, C. Duran, J. Photochem. Photobiol. A: Chem. 198 (2008) 1–6.
[7] N. Daneshvar, D. Salari, A.R. Khataee, J. Photochem. Photobiol. A: Chem. 162 (2004) 317–322.
[8] G. Colón, M.C. Hidalgo, J.A. Navío, E.P. Melián, O.G. Díaz, J.M. Rodríguez, Appl. Catal. B: Environ. 83 (2008) 30–38.
[9] S. Sakthivel, B. Neppolian, M.V. Shankar, B. Arabindoo, M. Palanichamy, V. Murugesan, Sol. Energy Mater. Sol. Cells 77 (2003) 65–82.
[10] N. Serpone, P. Maruthamuthu, P. Pichat, E. Pelizzetti, H. Hidaka, J. Photochem. Photobiol. A: Chem. 85 (1995) 247–255.
[11] G. Marcì, V. Augugliaro, M.J. López-Munõz, C. Martín, L. Palmisano, V. Rives, M. Schiavello, R.J.D. Tilley, A.M. Venezia, J. Phys. Chem. B 105 (2001) 1033–1040.
[12] G. Marcì, V. Augugliaro, M.J. López-Munõz, C. Martín, L. Palmisano, V. Rives, M. Schiavello, R.J.D. Tilley, A.M. Venezia, J. Phys. Chem. B 105 (2001) 1026–1032.
[13] C. Shifu, Z. Wei, L. Wei, Z. Sujuan, Appl. Surf. Sci. 255 (2008) 2478–2484.
[14] S. Sakthivel, S.U. Geissen, D.W. Bahnemann, V. Murugesan, A. Vogelpohl, J. Photochem. Photobiol. A: Chem. 148 (2002) 283–293.
[15] J. Nayak, S.N. Sahu, J. Kasuya, S. Nozaki, Appl. Surf. Sci. 254 (2008) 7215–7218.
[16] C. Wang, J.C. Zhao, X.M. Wang, B.X. Mai, G.Y. Sheng, P.A. Peng, J.M. Fu, Appl. Catal. B: Environ. 39 (2002) 269–279.
[17] M. Zhang, T. An, X. Hu, C. Wang, G.Y. Sheng, J. Fu, Appl. Catal. A: Gen. 260 (2004) 215–222.
[18] M. Zhang, G.Y. Sheng, J.M. Fu, T. An, X.M. Wang, X. Hu, Mater. Lett. 59 (2005) 3641–3644.
[19] T. An, M. Zhang, X.M. Wang, G.Y. Sheng, J.M. Fu, J. Chem. Technol. Biotechnol. 80 (2005) 251–258.
[20] C. Wang, X. Wang, B.-Q. Xu, J. Zhao, B. Mai, P.A. Peng, G.Y. Sheng, J. Fu, J. Photochem. Photobiol. A: Chem. 168 (2004) 47–52.
[21] A. Hamrouni, H. Lachheb, A. Houas, Mater. Sci. Eng. B 178 (2013) 1371–1379.
[22] A. Dodd, A. McKinley, T. Tsuzuki, M. Saunders, J. Eur. Ceram. Soc. 29 (2009) 139–144.
[23] I.L. Validzić, T.D. Savić, R.M. Krsmanović, D.J. Jovanović, M.M. Novaković, M.Č. Popović, M.I. Čomor, Mater. Sci. Eng. B 177 (2012) 645–651.
[24] Y. Wang, L. Cai, Y. Li, Y. Tang, C. Xie, Physica E 43 (2010) 503–509.
[25] X. Zhao, W. Yao, Y. Wu, S. Zhang, H. Yang, Y. Zhu, J. Solid State Chem. 179 (2006) 2562–2570.
[26] G. Huang, Y. Zhu, Mater. Sci. Eng. B 139 (2007) 201–208.
[27] G. Huang, C. Zhang, Y. Zhu, J. Alloys Compd. 432 (2007) 269–276.
[28] J. Lin, J. Lin, Y. Zhu, Inorg. Chem. 46 (2007) 8372–8378.
[29] H. Fu, J. Lin, L. Zhang, Y. Zhu, Appl. Catal. A: Gen. 306 (2006) 58–67.
[30] R. Shi, Y. Wang, D. Li, J. Xu, Y. Zhu, Appl. Catal. B: Environ. 100 (2010) 173–178.
[31] D. He, X. Zhang, T. Xie, J. Zhai, H. Li, L. Chen, L. Peng, Y. Zhang, T. Jiang, Appl. Surf. Sci. 257 (2011) 2327–2331.
[32] D. Li, R. Shi, C. Pan, Y. Zhu, H. Zhao, CrystEngComm 13 (2011) 4695–4700.
[33] M.-J. Kim, Y.-D. Huh, Mater. Res. Bull. 45 (2010) 1921–1924.
[34] W. Zhao, X. Song, G. Chen, S. Sun, J. Mater. Sci. 44 (2009) 3082–3087.
[35] J. Bi, L. Wu, Z. Li, Z. Li, Z. Ding, X. Wang, X. Fu, J. Alloys Compd. 480 (2009) 684–688.
[36] S. Lin, J. Chen, X. Weng, L. Yang, X. Chen, Mater. Res. Bull. 44 (2009) 1102–1105.
[37] T. Montini, V. Gombac, A. Hameed, L. Felisari, G. Adami, P. Fornasiero, Chem. Phys. Lett. 498 (2010) 113–119.
[38] M. Mancheva, R. Iordanova, Y. Dimitriev, J. Alloys Compd. 509 (2011) 15–20.
[39] K.M. Garadkar, L.A. Ghule, K.B. Sapnar, S.D. Dhole, Mater. Res. Bull. 48 (2013) 1105–1109.
[40] M. Koizumi, Y. Yamamoto, Y. Ito, M. Takano, T. Enami, E. Kamata, R. Hasegawa, J. Toxicol. Sci. 26 (2001) 299–311.
[41] M.A. Butler, J. Appl. Phys. 48 (1977) 1914–1920.
[42] A.M. Roy, G.C. De, N. Sasmal, S.S. Bhattachayya, Int. J. Hydrogen Energy 20 (1995) 627–630.
[43] P. Wardman, J. Phys. Chem. Ref. Data 18 (1989) 1637–1756.
[44] B. Ohtani, Y. Ogawa, S.-I. Nishimoto, J. Phys. Chem. B 101 (1997) 3746–3752.
[45] A. Di Paola, M. Bellardita, R. Ceccato, L. Palmisano, F. Parrino, J. Phys. Chem. C 113 (2009) 15166–15174.